CHARACTERIZATION OF MAGNETOSTATIC WAVE DEVICES BY BRILLOUIN LIGHT SCATTERING

G. Srinivasan, J. G. Booth, and C. E. Patton.

Abstract - Brillouin light scattering (BLS) has been used for direct detection of backward volume wave (BVW) excitations in yttrium iron garnet (YIG) films in magnetostatic wave devices. The measurements were carried out on delay line structures and on a signal-to-noise enhancer device. With an applied field parallel to the film plane and perpendicular to the stripline, backward volume waves are excited in the YIG film by the stripline power. Using the BLS technique, the BVW excitations in the YIG film were observed over the frequency range 2-4 GHz. The observed BVW band limits are in reasonable agreement with theory. There is very good agreement between the experimental and the theoretical dispersion for the BVW excitations. The scattering was found to be rather weak over the BVW passband, but did reveal considerable structure.

Introduction

Magnetostatic wave (MSW) devices such as delay lines, power limiters, and signal-to-noise enhancers are used for signal processing at microwave frequencies [1]. In these devices, magnetostatic waves are excited in a yttrium iron garnet (YIG) film by an external microwave signal. Direct observation of such MSW excitations is possible with the technique of Brillouin light scattering (BLS). This technique has been used to observe magnetostatic surface waves and parametric spin waves excited in YIG films in a signal-to-noise enhancer device [2], [3]. It was possible to obtain quantitative information on energy flow profile, magnon dispersion, and spin wave instability processes [4]. Results of recent light scattering studies on backward volume waves (BVW) in YIG film MSW devices are presented here.

The BLS measurements were performed on (i) a signal-to-noise enhancer MSW device with a stripline on an alumina ground plane [5], [6], and (ii) delay line device structures in which stripline transducers are deposited onto silica or sapphire substrates. In both cases, one has a YIG film in contact with the stripline. With an appropriate in-plane static magnetic field applied perpendicular to the stripline, backward volume waves are excited in the YIG film by the stripline power.

In light scattering, the interaction between the incident laser light and the magnetic excitations in the YIG film gives rise to frequency shifted scattered light. The Brillouin spectrum, i.e., the intensity vs. frequency profile for the scattered light, is obtained by analyzing the scattered light with a high contrast Fabry-Perot interferometer. One observes intensity peaks at frequencies corresponding to the magnetic excitations. In this study, the BLS technique was used to observe BVW excitations and to measure intensity vs. field profiles and magnon dispersion. The BVW band limits and dispersion curves were found to be in agreement with the theoretical predictions.

Manuscript received March 1, 1987.

G. Srinivasan and C. E. Patton are with the Department of Physics, Colorado State University, Fort Collins, CO 80523.

J. G. Booth is with the Department of Pure and Applied Physics, University of Salford, Salford M5 4WT, UK. This work was performed while Professor Booth was a Visiting Professor at Colorado State University.

This work was supported by the Electromagnetics Directorate of the Rome Air Development Center, Hanscom Air Force Base, MA., Contract # F19628-85-K-0002.

Backward Volume Waves

There are two types of magnetic wave excitations for in-plane magnetized slabs, backward volume waves (BVW) and surface waves [7]. Work on surface waves has been reported previously [2]-[4]. The magnon dispersion for the volume waves is shown schematically in Fig. 1 for propagation parallel to the applied magnetic field. The frequency f_k is shown as a function of wavenumber for the various BVW dispersion branches. The upper and lower frequency limits for the BVW excitations are indicated by f_B and f_H, respectively. These limits are given by

$$f_B = \gamma \left[H \left(H + 4\pi M_s \right) \right]^{1/2} \qquad (1)$$

and

$$f_H = \gamma H, \qquad (2)$$

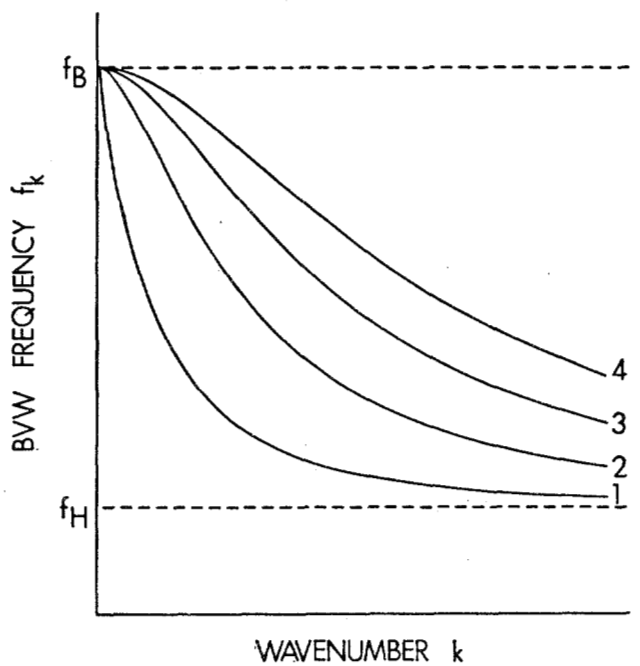

Fig. 1. Schematic frequency vs. wavenumber dispersion branches for backward volume waves (BVW) propagating parallel to the in-plane applied field in thin films. The frequencies f_H and f_B correspond to the lower and upper limits for BVW excitations.

where H is the in-plane applied field, $4\pi M_s$ is the saturation induction, and $2\pi\gamma$ is the gyromagnetic ratio.

The dispersion shown in Fig. 1 is for the BVW excitations with the in-plane wavevector $\bar{k}$ along $\bar{H}$. For large k, the excitation profile for the volume waves across the film thickness corresponds to a set of standing waves and the magnon wavenumber perpendicular to the film plane is quantized according to $k_\perp = n\pi/S$, where n = 1,2.., and S is the film thickness. Each branch in Fig. 1 corresponds to a particular $k_\perp$ solution. The dispersion branches all have negative slope, so that the group velocity $\partial f_k/\partial k$ is generally negative in the midband region, $f_H < f_k < f_B$. This negative group velocity is the basic reason for the "BVW" or "backward volume wave" nomenclature.

The objective of this BLS study was to detect directly the BVW excitations which are present in YIG films in MSW device structures and to measure the dispersion properties and scattering profiles for these excitations in actual device configurations.

The Device Structures

The signal-to-noise enhancer (SNE) and delay line (DL) structures which were used for the BLS investigations are shown schematically in Fig. 2. The SNE device in Fig. 2(a) consists of a stripline transducer on an alumina ground plane [5], [6]. A YIG film on a gadolinium gallium garnet (GGG) substrate is in contact with the stripline. In the delay line type device in Fig. 2(b), the actual device configuration involved two different structures, one with a sapphire substrate and relatively narrow (22 μm) stripline transducers, and one with a silica substrate and relatively broad (560 μm) transducers. These substrates were mounted in an open support structure for which the metal ground plane was removed over the active region of the device. This open structure was proved to be very useful in order to conveniently access the film with the laser beam for the BLS

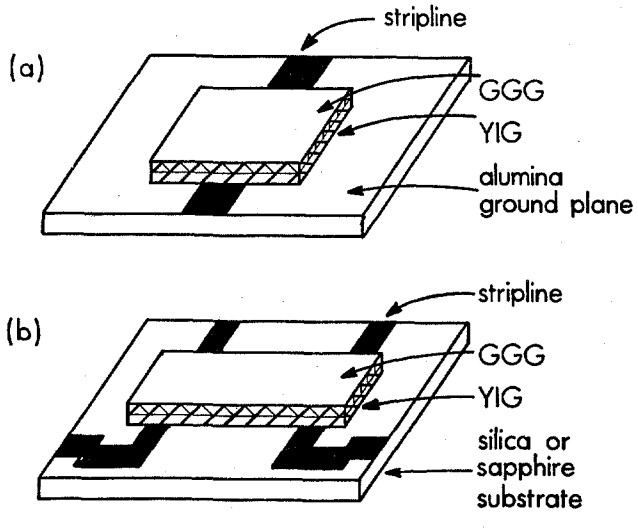

Fig. 2. Diagram showing (a) a signal-to-noise enhancer (SNE) device structure and (b) a delay line (DL) magnetostatic wave device structure. The yttrium iron garnet film (YIG), the gadolinium gallium garnet (GGG) substrate for the YIG, the stripline transducer(s), and the ground plane support structures are indicated.

measurements, even though there was some degradation in the microwave impedance matching characteristics of the overall device.

The stripline dimensions and the magnetic parameters for the YIG films used with the various devices are given in Table I. The effective $4\pi M_s$ and γ values were determined from ferromagnetic resonance for in-plane and out-of-plane fields. The film thickness were determined by interference techniques, courtesy of Westinghouse and Hewlett Packard.

Table I

Stripline width (w) and YIG film material parameters (thickness S, effective saturation induction $4\pi M_s$, and reduced gyromagnetic ratio γ) for the signal-to-noise (SNE) device and the delay line (DL) device structures on sapphire and silica.

Device	stripline width w (μm)	film thickness S (μm)	saturation induction $4\pi M_s$ (kG)	reduced γ (GHz/kOe)
SNE	30	26.6	1.84	2.80
DL				
(a) Sapphire	22	20.0	1.75	2.82
(b) Silica	560			

In order to excite backward volume waves in the devices, it is necessary to apply a d.c. magnetic field parallel to the YIG film plane and perpendicular to the stripline. For suitable bias fields, volume waves are excited in the YIG film by the stripline power. These BVW excitations propagate parallel to $\bar{H}$ and carry power away from the stripline. In the SNE device, one observes attenuation of the input microwave power when BVW excitations are present. In the DL device, BVW excitations in the YIG film result in coupling of microwave power to the output transducer.

Typical data on the applied field dependence of the measured output power are shown in Fig. 3 for the DL device on sapphire, an excitation frequency of 4 GHz, and an input power of 40 mw. These data will also be useful for comparison with the results of BLS measurements described in subsequent sections. For fixed frequency measurements, as in Fig. 3, it is convenient to think in terms of a field range, $H_B < H < H_H$, for which BVW excitations are supported. The lower field limit H_B is simply the value of H from (1) for $f = f_B$. H_H is similarly obtained from (2) with $f = f_H$. These field limits are indicated in Fig. 3 along with the microwave data for the DL device.

The microwave output power vs. field profile in Fig. 3 does show a reasonable correspondence to the BVW band, but with several qualifications. First, the power drops off rather rapidly for $H > H_B$. Second, there is no pronounced cutoff at $H = H_H$ as one might expect. This is due, presumably, to the drop in coupling for the higher wavenumber BVW modes as the field approaches H_H. Third, a very strong coupling is evident for fields somewhat below H_B. The large peak in intensity for applied fields below the low field BVW band edge may be due to surface waves excited in the YIG film [4].

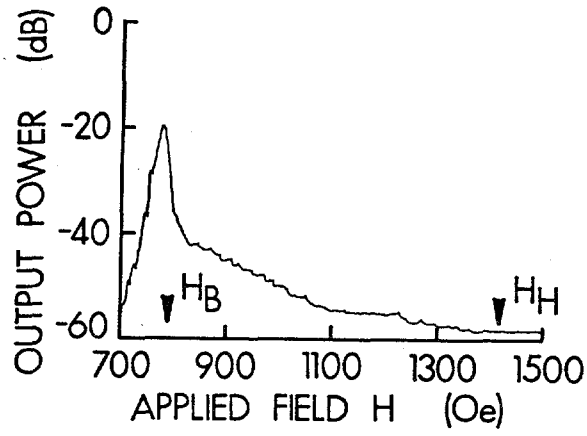

Fig. 3. Variation of the measured microwave output power with the applied field at 4 GHz in the DL device structure on sapphire. The input power was 40 mw. The bias field was parallel to the YIG film plane and was perpendicular to the portion of the stripline in contact with the YIG film. The field limits for the BVW excitations , H_B and H_H, are indicated.

It is evident that microwave data leave many open questions about the pertinent device physics. One has no direct way to access the MSW modes which give rise to the observed device properties. Previous work [2]-[4] has shown that BLS techniques can be used to complement microwave data on MSW devices in a meaningful way by providing specific information on dispersion, coupling power vs. wavenumber, and other properties of the magnetic signals. The results of light scattering studies on the BVW excitations in these device structures are presented in the following sections.

Experiment

In Brillouin light scattering, the incident laser light is focused onto the material of interest and the scattered light from the material is collected for frequency analysis. The interaction with magnons of frequency f within the material gives rise to a frequency shift of ± f for the scattered light. One can measure the intensity vs. frequency profile for the scattered light with a Fabry-Perot interferometer [8]. The Brillouin spectrum thus obtained shows intensity peaks at frequencies corresponding to the magnetic excitations which are present in the material.

Since momentum is also conserved in the scattering process, the magnon wavevector $\bar{k}$ is defined by the scattering geometry. In the present study, we are interested in the direct detection of volume waves with wavenumbers over the range $0 < k < 10^4$ cm^{-1}. A forward scattering configuration, such as shown in Fig. 4, is essential for the observation of such excitations. The scattering set-up is shown in Fig. 4(a) and the scattering geometry in terms of wavevectors is shown in Fig. 4(b). Figure 4(c) shows the details of the diaphragm and aperture arrangement for magnon wavevector selection.

Consider first the forward scattering set-up in Fig. 4(a). Incident laser light is focused onto the YIG film through a hole in the alumina ground plane in the SNE device. Such an access hole was not needed for the

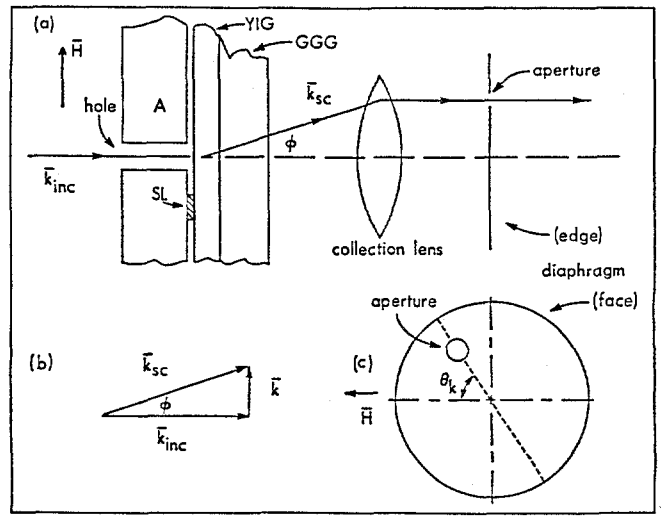

Fig. 4. Diagram showing (a) the scattering geometry used for direct detection of BVW excitations in the SNE device consisting of an alumina ground plane (A), a stripline (SL), and a yttrium iron garnet film (YIG) on a gadolinium gallium garnet (GGG) substrate; (b) the scattering geometry in terms of the incident ($\bar{k}_{inc}$), scattered ($\bar{k}_{sc}$), the magnon ($\bar{k}$) wavevectors; and (c) the diaphragm and aperture arrangement for wavenumber selection. The parameters θ_k and ϕ are defined in the text.

DL device measurements since the substrates were of transparent silica and sapphire. The limit on the accessible k - values is determined by the size of the collection lens. With the 50 mm focal length, f/1.4 lens used in this work, magnons with k - values over the range $0 - 4 \times 10^4$ cm^{-1} can be observed. Scattering due to magnons with specific k - values can be examined selectively by placing an aperture on the blocking diaphragm in Fig. 4(a) [9]. The angle ϕ controls the in-plane wavenumber for the magnons contributing to scattering. The direction of the in-plane wavevector relative to the applied field is controlled by the aperture orientation, as indicated in Fig. 4(c), where θ_k denotes the angle between $\bar{k}$ and $\bar{H}$.

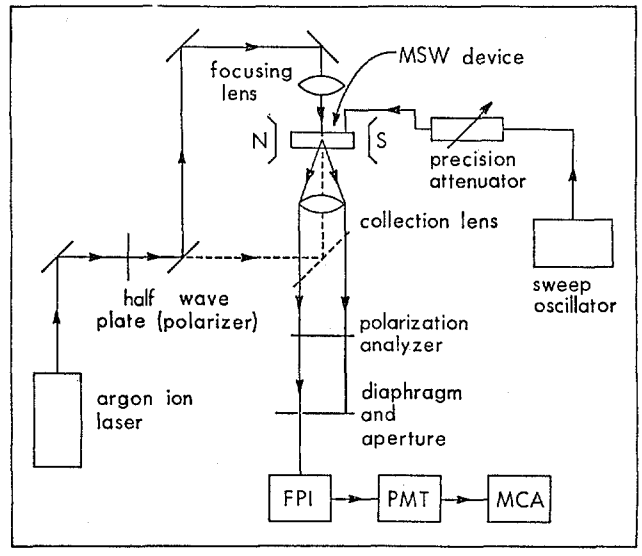

Fig. 5. Schematic diagram showing the Brillouin light scattering spectrometer.

Figure 5 shows the overall layout of the spectrometer. Laser light (λ = 5145 A) is linearly polarized with a half wave plate and is directed towards the YIG film in the device. Initially, a back scattering configuration, indicated by the dotted line in Fig. 5, is used to position the YIG film at the focus of the collection lens. The forward scattered light passes through a polarization analyzer and is analyzed with a high contrast multipass Fabry-Perot interferometer (FPI). The photon counting system consists of a low dark count photomultiplier tube (PMT). The Brillouin spectrum is recorded with a multichannel analyzer (MCA). The in-plane bias field is provided by a Helmholtz pair. A microwave sweep oscillator was used for the stripline excitation over the frequency range from 2 to 4 GHz.

A representative Brillouin spectrum for SNE device structure is shown in Fig. 6. These data are for an excitation frequency of 4 GHz and input power of 40 mw. An in-plane static field of 900 Oe was applied perpendicular to the stripline. This bias field is well within the field limits $H_B - H_H$ for volume waves at 4 GHz. The spectrum in Fig. 6 was obtained with no wavenumber selective aperture in place so that scattering due to all possible BVW excitations with $k < 4 \times 10^4$ cm^{-1} could be detected.

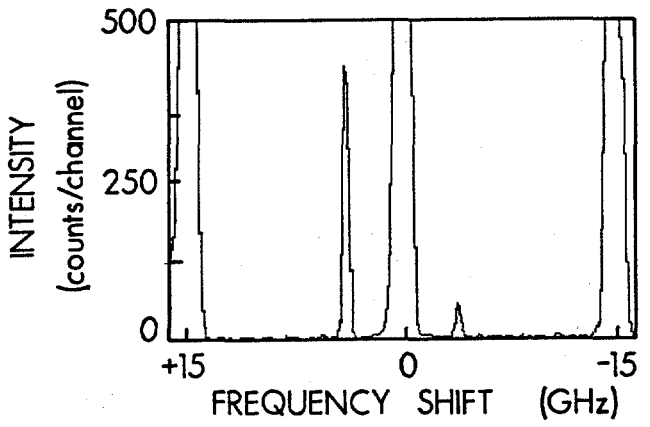

Fig. 6. Brillouin spectrum for BVW excitations at 4 GHz in the SNE device. The input power was 40 mw and the bias field was 900 Oe.

The two peaks at ± 4 GHz in the spectrum of Fig. 6 correspond to the BVW excitations generated in the device. The strong central peak at "0" and the satellite peaks at ± 15 GHz correspond to the central and adjacent interference order peaks for the laser line frequency. Spectra similar to the example in Fig. 6, but with various wavevector selection apertures in place and as a function of field, can be used to obtain quantitative information on the BVW excitations in the device under study.

Some comments on the magnon peak intensities are in order here. At the outset of these investigations, it was anticipated that the BLS intensity would be stronger for anti-Stokes scattering (destruction of pumped magnons and an up-shift in the scattered light frequency) than for Stokes scattering (creation of a new BVW magnon and a down-shift in the scattered light frequency). The relative peak intensities in Fig. 6 appear to support this expectation. Upon closer examination, however, it was found that the relative intensities for Stokes and anti-Stokes scattering is very sensitive to the way in which the scattered light is collected. When the collection lens focus is moved from a film region near the YIG-GGG interface (as for Fig. 6) to a region near the YIG-air/ stripline interface, the Stokes peak become more intense than the anti-Stokes peak! When the collection optics is focused in the middle of the YIG film, the two intensities are approximately equal. One possible explanation of equal intensities is that under microwave excitation, the ground state and the excited state of the magnon system are equally populated and give rise to equal scattering intensities for magnon creation and destruction. These points require further investigation.

Magnon Dispersion and Intensity Profiles

In addition to simply observing magnon peaks in the BLS spectra at appropriate frequencies, it is possible to measure the dispersion for the excitations and obtain BVW intensity profiles in MSW device configurations. Selected results for such experiments are presented in this section.

Dispersion curves of BVW field position at fixed frequency, $f = f_k$, vs. wavenumber k are obtained from intensity vs. field data for specific aperture selected k - values. The aperture selection scheme, following the discussion given above and the diagrams of Fig. 4, utilized a 50 μm diameter aperture positioned at various places in the aperture plane, as indicated in Fig. 4(a) and 4(c). Figure 7 shows representative profile data for an on-axis aperture, corresponding to k = 0, and scattering from the SNE device at 4 GHz. One would expect a peak in the scattering at $H = H_B$ for k = 0. The observed peak, some 10 Oe higher, is in reasonable agreement with this expectation. The field width for the "resonance" like profile in Fig. 7 is related to the spread in k - values due to the finite size of the aperture.

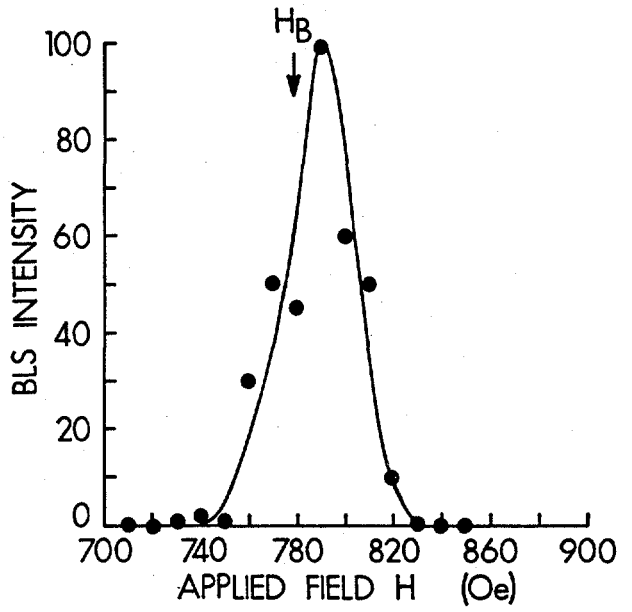

Fig. 7. Brillouin light scattering intensity vs. applied field for the SNE device at 4 GHz with the wavenumber selective aperture on the diaphragm in Fig. 4(c) on axis, corresponding to zero magnon wavenumber. The theoretical field position for BVW excitations with zero wavenumber, H_B, is indicated.

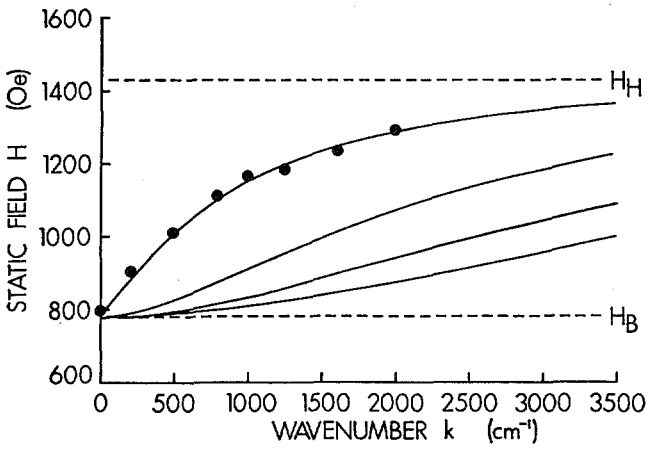

Fig. 8. Data on field vs. wavenumber for the BVW excitations propagating parallel to the applied field in the SNE device at 4 GHz. The solid lines represent theoretical field vs. wavenumber dispersion curves for the first four BVW branches.

By utilizing a series of profiles for different aperture positions, one may construct dispersion curves for the device under study. Typical results, again for the SNE device, are shown in Fig. 8. The data points represent the peak positions in field, as from Fig. 7, versus wavenumber k. The k - values were controlled simply by positioning the aperture a larger distance away from the optic axis [Fig. 4(c)]. The data in Fig. 8 are for a θ_k- value of zero, such that $\tilde{k}$ is parallel to $\tilde{H}$.

The solid lines in Fig. 8 show the theoretical dispersion curves for BVW excitations based on the well-known theory of Damon-Eshbach [7]. Curves are shown for the first four BVW branches. These dispersion curves of field vs. wavenumber are essentially "flipped over" versions of the frequency vs. wavenumber curves in Fig. 1. Figure 8 shows that the BLS measurements track the expected dispersion for the lowest order BVW dispersion branch almost perfectly. It was not possible to obtain data points corresponding to the higher order BVW branches. The scattering for these modes was too weak for meaningful measurements.

The final MSW device result which is unique to light scattering concerns profiles of scattering intensity vs. field for no wavenumber selective aperture in the collection optics. Such profiles are somewhat analagous to the microwave power vs. field curve shown in Fig. 3, except that one is probing the actual modes which carry the power.

Profiles of this sort are shown in Fig. 9 for the two different DL device substrate/ transducer configurations. The profile in Fig. 9(a) is for the sapphire substrate with 22 μm wide transducers, while Fig. 9(b) is for silica and 560 μm transducers. As discussed earlier, the range of MSW wavenumbers which are accessed with no aperture in place is $0 < k < 4 \times 10^4$ cm^{-1}. Both profiles in Fig. 9 are for 4 GHz microwave excitation and an input power of 40 mw. The profiles were obtained by the continuous field sweep technique described in Ref. [10].

The passband in field for the BVW modes, $H_B < H < H_H$, is somewhat more evident for the light scattering data in Fig. 9 than for the microwave power profiles given earlier, even though the actual scattering is rather weak. The scattering in Fig. 9(a) falls off somewhat less rapidly for $H > H_B$, compared to the fall off in Fig. 9(b). This is attributed to a stronger coupling to the high k modes for the narrow 22 μm stripline transducer than for the wide 560 μm transducer. The fact that the scattering over the entire $H_B < H < H_H$ passband is rather weak is probably due to the poor coupling, overall, between the transducers and the YIG. Such weak coupling is attributed to YIG - transducer mismatch, the open nature of the structure with no bona fide ground plane, etc.

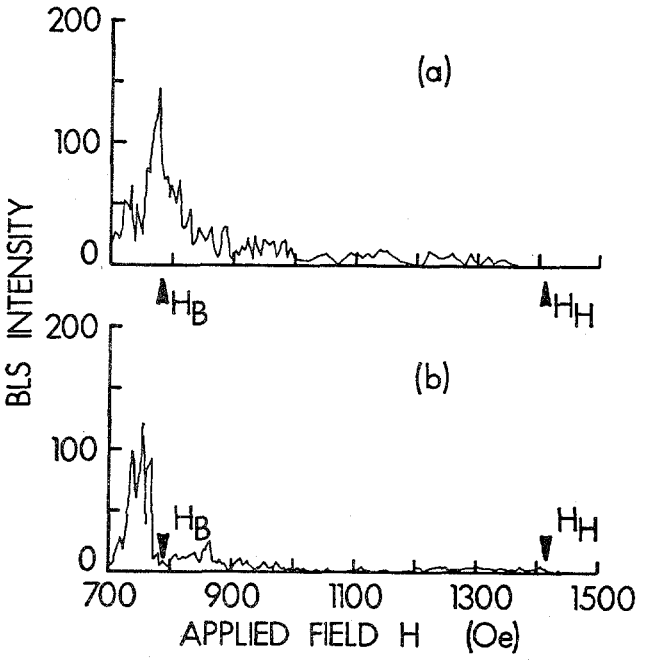

Fig. 9. BLS intensity profiles at 4 GHz and 40 mw input power for the DL device structures on (a) sapphire and (b) silica. The field limits for BVW excitations, H_B and H_H, are indicated.

The profiles in Fig. 9 also reveal considerable structure. It is to be noted that this structure is real and completely reproducible. The structure in the passband region is most likely due to the preferential coupling to BVW excitations at specific wavelengths. The structure is somewhat finer for the narrow transducer [Fig. 9(a)] than for the wide transducer [Fig. 9(b)] as one would expect. The large intensities and pronounced structure below H_B are attributed to surface magnetostatic waves [4].

Summary and Conclusion

The above results demonstrate the utility of the BLS technique for the study of BVW excitations and the characterization of two different types of MSW devices. It was shown possible to utilize open support structures in combination with transparent substrates to observe forward scattering on MSW signals and to measure dispersion and energy flow profiles.

Acknowledgements

The authors gratefully acknowledge Dr. J. D. Adam,

Westinghouse Research and Development Center, Pittsburgh, Pennsylvania and Dr. W. Ishak, Hewlett Packard Laboratories, Palo Alto, California for providing the device structures and the YIG films used in this work, and the reviewer for his comments on the intensities of Stokes/ anti-Stokes magnon peaks.

References

[1] J. C. Sethares, Proc. 1981 Rome Air Development Center Microwave Magnetics Technology Workshop, Hanscom, Massachusetts, June 10-11, 1981, RADC-TR-83-15, January, 1983.

[2] G. Srinivasan and C. E. Patton, IEEE Trans. Magn. 21, 1797 (1985).

[3] G. Srinivasan and C. E. Patton, Appl. Phys. Lett. 47, 761 (1985).

[4] G. Srinivasan, C. E. Patton, and P. R. Emtage, J. Appl. Phys. 61, 2318 (1987).

[5] J. D. Adam, IEEE Trans. Magn. 16, 1068 (1980).

[6] J. D. Adam and S. N. Stitzer, Appl. Phys. Lett. 36, 485 (1980).

[7] R. W. Damon and J. R. Eshbach, J. Phys. Chem. Solids, 19, 308 (1961).

[8] J. R. Sandercock, Top. Appl. Phys. 51, 173 (1982).

[9] W. Wettling, W. D. Wilber, P. Kabos, and C. E. Patton, Phys. Rev. Lett. 51, 1680 (1983).

[10] W. D. Wilber, W. Wettling, P. Kabos, C. E. Patton, and W. Janz, J. Appl. Phys. 55, 2533 (1984).